

### Low resolution scans can provide a sufficiently accurate, costand time-effective alternative to high resolution scans for 3D shape analyses

Ariel E Marcy Corresp., 1, Carmelo Fruciano 2, Matthew J Phillips 3, Karine Mardon 4,5, Vera Weisbecker 1

Corresponding Author: Ariel E Marcy Email address: a.marcy@uq.edu.au

**Background.** Advances in 3D shape capture technology have made powerful shape analyses, such as geometric morphometrics, more feasible. While the highly accurate micro-computed tomography ( $\mu$ CT) scanners have been the "gold standard," recent improvements in 3D surface scanner resolution may make this technology a faster, portable, and cost-effective alternative. Several studies have already compared the two devices but all use relatively large specimens such as human crania. Here we perform shape analyses on Australia's smallest rodent species to test whether a 3D scanner produces similar results to a  $\mu$ CT scanner.

**Methods.** We captured 19 delicate mouse crania with a  $\mu$ CT scanner and a 3D scanner for geometric morphometrics. We ran multiple Procrustes ANOVAs to understand how variation due to scan device compared to other sources such as biologically relevant variation and operator error. We quantified operator error as levels of variation and repeatability. Further, we tested if the different devices performed differently at classifying individuals based on sexual dimorphism. Finally, we inspected scatterplots of principal component analysis (PCA) scores for non-random patterns.

**Results.** In all Procrustes ANOVAs, regardless of factors included, differences between individuals contributed the most to total variation. The PCA plots reflect this in how the individuals are dispersed. Including only the symmetric component of shape increased the biological signal relative to variation due to device and due to error. 3D scans showed a higher level of operator error as evidenced by a greater spread of their replicates on the PCA, a higher level of multivariate variation, and a lower repeatability score. However, the 3D scan and  $\mu$ CT scan datasets performed identically in classifying individuals based on intra-specific patterns of sexual dimorphism.

**Discussion.** Compared to  $\mu$ CT scans, we find that even low resolution 3D scans of very small specimens are sufficiently accurate to classify intra-specific differences. We also make three recommendations for best use of low resolution data. First, we recommend that extreme caution should be taken when analyzing the asymmetric component of shape variation. Second, using 3D scans generates more random error due to increased landmarking difficulty, therefore be conservative in landmark choice and avoid multiple operators. Third, using 3D scans introduces a source of systematic error relative to  $\mu$ CT scans, therefore we recommend not to combine them when possible and especially in studies expecting little biological variation. Our findings support increased use of low resolution 3D scans for most

<sup>&</sup>lt;sup>1</sup> School of Biological Sciences, University of Queensland, Brisbane, Queensland, Australia

<sup>2</sup> Institut de biologie de l'Ecole normale supérieure, Ecole normale supérieure, Université Paris, Paris, France

<sup>&</sup>lt;sup>3</sup> School of Earth, Environmental and Biological Sciences, Queensland University of Technology, Brisbane, Queensland, Australia

 $<sup>^{4}</sup>$  Centre for Advanced Imaging, University of Queensland, Brisbane, Queensland, Australia

<sup>&</sup>lt;sup>5</sup> National Imaging Facility, University of Queensland, Brisbane, Queensland, Australia



morphological studies; they are likely also applicable to low resolution scans of large specimens made in a medical CT scanner. As most vertebrates are relatively small, we anticipate our results to bolster more researchers designing affordable large scale studies on small specimens with 3D surface scanners.



1 Low resolution scans can provide a sufficiently accurate, cost- and time-effective 2 alternative to high resolution scans for 3D shape analyses 3 4 Authors: Ariel E. Marcy<sup>1</sup>, Carmelo Fruciano<sup>2</sup>, Matthew J. Phillips<sup>3</sup>, Karine Mardon<sup>4,5</sup>, Vera 5 Weisbecker<sup>1</sup> 6 1 School of Biological Sciences, University of Queensland, Brisbane, Australia 7 8 2 Institut de biologie de l'Ecole normale supérieure (IBENS), Ecole normale supérieure, 9 CNRS, INSERM, PSL Université Paris, Paris, France 10 3 School of Earth, Environmental and Biological Sciences, Queensland University of 11 Technology, Brisbane, Australia 12 4 Centre for Advanced Imaging, University of Queensland, Brisbane, Australia 13 5 National Imaging Facility, University of Queensland, Brisbane, Australia 14 15 Corresponding Author: 16 Ariel E. Marcy 17 a.marcy@uq.edu.au



18 Abstract 19 **Background.** Advances in three-dimensional (3D) shape capture technology have made 20 powerful shape analyses, such as geometric morphometrics, more feasible. While the highly 21 accurate micro-computed tomography (µCT) scanners have been the "gold standard," recent 22 improvements in 3D surface scanner resolution may make this technology a faster, more 23 portable, and cost-effective alternative. Several studies have already compared the two scanning 24 devices but all use relatively large specimens such as human crania. Here we perform shape 25 analyses on Australia's smallest rodent species to test whether a 3D surface scanner produces 26 similar results to a µCT scanner. **Methods.** We captured 19 delicate mouse crania with a  $\mu$ CT scanner and a 3D surface scanner 27 28 for geometric morphometrics. We ran multiple Procrustes ANOVAs to understand how variation 29 due to scan device compared to other sources of variation such as biologically relevant sources 30 and operator error. We quantified operator error as levels of variation and repeatability. Further, 31 we tested whether different devices performed differently at classifying individuals based on a 32 biological source of variation (sexual dimorphism). Finally, we inspected scatterplots of principal 33 component analysis (PCA) scores for non-random patterns. 34 **Results.** In all Procrustes ANOVAs, regardless of factors included, differences between 35 individuals contributed the most to total variation. This is also reflected in the way individuals 36 disperse on the PCA plots. Including only the symmetric component of shape increased the 37 biological signal relative to variation due to device and due to error. 3D scans showed a higher 38 level of operator error as evidenced by a greater spread of their replicates on the PCA, a higher 39 level of multivariate variation, and a lower repeatability score. However, the 3D scan and µCT



40	scan datasets performed ide	ntically in class	ıfyıng ındıvıdual	ls based on smal	l intra-specific

41 differences (sexual dimorphism).

Discussion. Compared to μCT scans, we find that even very low resolution 3D scans of very small specimens are sufficiently accurate to capture variation at the level of interspecific differences for classification purposes. We also make three recommendations for best use of low resolution data. First, we recommend that extreme caution should be taken when analyzing the asymmetric component of shape variation. Second, using 3D scans generates more random error due to increased landmarking difficulty, therefore be conservative in landmark choice and avoid multiple operators. Third, using 3D scans introduces a source of systematic error relative to μCT scans, therefore we recommend not to combine them when possible and especially in studies where little biological variation is expected. Our findings support increased use of low resolution 3D images for most morphological studies; they are likely applicable to low resolution scans of large specimens made in a medical CT scanner, for example. As most vertebrates are relatively small, we anticipate our results to bolster more researchers designing affordable large scale studies on small specimens with 3D surface scanners.

56 Introduction

An organism's shape reveals many facets of its biology, including its evolution, ecology, and functional morphology. In the past three decades, geometric morphometrics has revolutionized the field of shape research with better analysis and visualization of shape complexity (Rohlf & Marcus 1993; Zelditch et al. 2012). As imaging technology continues to advance, three-dimensional (3D) data have become extremely common in geometric morphometric studies, especially in the cases in which 2D data poorly represent the actual 3D object (Buser et al. 2017;





63	Cardini 2014; Fruciano 2016; Reig 1996). 3D capture methods include very high resolution yet
64	high cost and time-intensive options like micro-computed tomography ( $\mu$ CT) scanning. In
65	contrast, 3D surface scanning offers lower acquisition costs and faster scanning, but has the
66	disadvantage of generally lower resolution, which limits its use on very small specimens (Fig. 1).
67	For confident use of surface scans in small specimens, it is therefore important to assess the
68	measurement error introduced by choosing a 3D surface scanner for geometric morphometrics.
69	
70	Most vertebrates would be considered small, for example about two thirds of mammals are
71	below 10kg (Weisbecker & Goswami 2010), which would translate to small skeletal specimens.
72	Therefore, morphometric studies proposing large sample sizes must be very well funded to use a
73	$\mu CT$ scanner or have a low-cost option, such as a 3D surface scanner. Previous studies have
74	compared $\mu\text{CT}$ scans to 3D surface scans, however, these were all done in large animals,
75	primarily primates (Badawi-Fayad & Cabanis 2007; Fourie et al. 2011; Katz & Friess 2014;
76	Robinson & Terhune 2017; Sholts et al. 2010; Slizewski et al. 2010). While these studies found
77	low error and high repeatability in 3D surface scans similar to $\mu CT$ scans, there was a suggestion
78	that higher error occurred in the sample's smaller specimens (Badawi-Fayad & Cabanis 2007;
79	Fourie et al. 2011). Other recent studies have conducted 3D geometric morphometric studies on
80	small vertebrate skulls but nearly all have relied exclusively on $\mu\text{CT}$ scanning (Cornette et al.
81	2013; Evin et al. 2011). The only exception we are aware of is (Munoz-Munoz et al. 2016),
82	which successfully used photogrammetry – a technique combining 2D photographs into a 3D
83	model – to analyze domestic mouse skulls, <i>Mus musculus domesticus</i> (Linnaeus, 1758).
84	Photogrammetry, like 3D surface scanning, is a low-cost alternative to $\mu CT$ and comes with its
85	own trade-offs in time and scan resolution (Katz & Friess 2014). Compared to the new





87

88

89

90

91

92

93

94

95

96

97

99

100

101

102

103

104

105

106

107

108

generation of blue light surface scanners, photogrammetry requires more time for image acquisition and for file processing (Katz & Friess 2014). A previous study on a single macaque specimen reported inconsistent levels of error across operators and scanners, which contributed to the lack of general pattern for differences across scanners/resolutions (Shearer et al. 2017). However, using an interspecific dataset, (Fruciano et al. 2017) reported higher repeatability for the higher resolution scans and 2.07-11.26% of total variance due to scan type (depending on device, operator and landmark set combination). We expect that small specimens would exacerbate any variation due to device and the interaction of device with other factors, such as landmark choice and operator. More work comparing these different methods –  $\mu$ CT scanning, 3D surface scanning, and photogrammetry – will allow researchers to make an informed decision. For example, for those with time constraints in museum collections, a fast 3D surface scanner may be the best option if the resolution is suitable for specimen size. 98 The lower resolution of 3D surface scanners may increase both random and systematic measurement error, which is exacerbated by small specimens because operators may have more difficulty identifying landmark locations (Arnqvist & Martensson 1998; Fruciano 2016). Random error increases variance without changing the mean; this "noise" dilutes biologically informative patterns and, in principle, decreases statistical power (Arnqvist & Martensson 1998; Fruciano 2016). By contrast, systematic error is non-randomly distributed, thus changing the mean and introducing bias to the data (Arnqvist & Martensson 1998; Fruciano 2016). Error assessment can be done with repeated measures of the same individuals (e.g. (Fruciano et al. 2017; Munoz-Munoz & Perpinan 2010; Robinson & Terhune 2017) or by comparison to a "gold standard" or ideal representation of the specimens (Fruciano 2016; Slizewski et al. 2010;





110

111

112

113

114

Williams & Richtsmeier 2003). Repeated measure designs can uncover this systematic error, for example, if one 3D capture method differs from another in a specific, non-random, pattern (Fruciano 2016; Fruciano et al. 2017). Furthermore, designs including repeated measures of the same individuals allow partitioning of variance into components, quantifying error due to scan device as compared to biologically-relevant sources of variation such as asymmetry (Fruciano 2016; Klingenberg et al. 2002; Klingenberg & McIntyre 1998).

115

116

117

118

119

120

121

122

123

124

125

126

127

128

129

130

In this study, we quantify the error introduced by studying specimens of a size at the very lower limits of commonly used portable surface scanners' resolution. This situation could also arise when using relatively large specimens, which are nonetheless at the lower limit of a medical CT scanner's resolution for example. We test whether the complex shape of very small specimens can be adequately captured using an HDI109 3D surface scanner with a stated resolution of 80 μm as compared to a μCT scanner with a resolution of 28 μm. To do so, we use the delicate mouse, Pseudomys delicatulus (Gould, 1842), one of the smallest rodents in the world with a 55-75 mm head-and-body length (Breed & Ford 2007). The miniscule *P. delicatulus* crania (~20mm) are at the edge of the HDI109 3D surface scanner's range thus providing an extreme test of this scanning device (Fig. 1, Fig. 2). First, we tested whether variation due to scanning device compared to other sources of variation (Fig. 2b). We also asked whether removing asymmetric variation, a common practice in morphological studies when asymmetry is not of interest, changed the results. Second, we tested whether the scanning devices differed in shape variance and in operator error (as measured by repeatability) (Fig. 2c). We also explored how including different types of landmarks impacted repeatability. Finally, we tested whether the



shape variation due to scanning device was large enough to impact a small study of intra-specific shape variation using the biologically relevant signal of sexual dimorphism (Fig. 2d).

134 Methods

#### **Data collection**

We selected 19 adult individuals, male and female, of *Pseudomys delicatulus* from the Queensland Museum in Brisbane, Australia (specimen numbers and sexes in Additional File 1: Table S1). The cranium from each individual was scanned at the Centre for Advanced Imaging at the University of Queensland in a μCT scanner (Siemens Inveon PET/CT scanner). The scanner was operated at 80 K hergy, 250 μA intensity with 540 projections per 360°, a medium-high magnification with bin 2 was applied, and 2000 ms exposure time. The samples were scanned at a nominal isotropic resolution of 28 μm. The data were reconstructed using a Feldkamp conebeam back-projection algorithm provided by an Inveon Acquisition workstation from Siemens (IAW version 2.1). Surface models were obtained using Mimics Research version 20.0.

Each cranium was also scanned by 3D LMI's Hear 09 blue light surface scanner with a resolution of 80 μm. For brevity, we will refer to this method as 3D scanning. For this method, the cranium was placed on a rotary table providing the scanner with 360 views. To capture the entire shape, the cranium was scanned in three different orientations: one ventral view with the cranium resting on the frontals and two dorsal views with the cranium tipped to each side, resting on an incisor, auditory bulla, and zygomatic arch. To assist others in replicating our HDI109 3D surface scanning on small specimens, we have included a Standard Operating Procedure with our settings (Additional File 2: Supplementary Methods).



After scanning every individual with both scan methods, we then replicated each 3D model three times so that each individual was represented by 6 replicates, giving a total sample of 114 3D models (Fig. 2a). Each 3D model was landmarked in Viewbox version 4.0 (dHAL software, Kifissia, Greece; www.dhal.com; (Polychronis et al. 2013). To capture shape, we placed 58 fixed landmarks, 145 semi-landmarks on curves, and 86 patch points (points that during sliding are allowed to slide across a 3D surface defined by the 3D model and semi-landmark borders) for a total of 289 points (Fig. 3, Additional File 3: Table S2). We used the template feature in Viewbox to semi-automate the placement of semi-landmarks on curves and to fully automate the placement of patch points. Our landmark design covered most important biological structures except for the zygomatic arch (Fig. 3); we avoided this fine structure because dehydration and loss of support from surrounding muscles during skeletonization almost certainly causes specimen preparation error (Schmidt et al. 2010; Yezerinac et al. 1992).

#### Data analysis

The landmark coordinates for all 114 3D models were aligned using a generalized Procrustes analysis followed by projection to the tangent space, as implemented in the R package *geomorph* (v. 3.0.5) (Adams 2016; Adams & Otarola-Castillo 2013). Generalized Procrustes analysis of each set of landmark coordinates removes differences in size, position, and orientation, leaving only shape variation (Rohlf & Slice 1990). Semi-landmarks and patches were permitted to slide along their tangent directions to minimize Procrustes distance between 3D models (Gunz et al. 2005). The resulting Procrustes tangent coordinates were used as shape variables in all subsequent shape analyses. All our statistical analyses were performed either in R





1//	(v. 3.3.3) using the R packages geomorph (v. 3.0.5) (Adams 2016; Adams & Otarola-Castillo
178	2013) and <i>Morpho</i> (v. 2.5.1) (Schlager 2017) or using MorphoJ (v. 1.06d) (Klingenberg 2011).
179	
180	First, asymmetry is a known source of variation within a sample (Klingenberg et al. 2002), so we
181	tested for it with MorphoJ's Procrustes ANOVA function and subsequently removed it (Fig. 2b).
182	Isolating the symmetric component of shape has been doon other 3D surface scanner studies
183	where operator and device error have been of the same magnitude as asymmetric error (Fruciano
184	et al. 2017). Variation due to asymmetry is more impacted by operator error because of its
185	smaller effect sizes compared to variation among individuals (Fruciano 2016; Fruciano et al.
186	2017; Klingenberg et al. 2010; Leamy & Klingenberg 2005). This suggests that low resolution
187	studies on asymmetry would be negatively impacted. For this reason, we performed most
188	subsequent analyses on the symmetric shape component, with a few exceptions performed for
189	comparison. We then performed a PCA on the symmetric shape variables to visualize the
190	variation between individuals, within scan method replicates, and between scan method
191	replicates. As an exploratory analysis, PCA can help intuitively visualize both random error
192	(greater spread of one scan method replicate compared to the other) and systematic error
193	(repeated pattern of one scan method shifting relative to another). However, further analyses are
194	necessary to quantify these sources of error.
195	
196	Second, our replicate design allowed us to assess whether an operator digitizing scans from one
197	device was more variable in landmark placement than when digitizing scans from the other
198	device (Fig. 2c). We did so by computing the Procrustes variance for each individual/device
199	combination. In <i>geomorph</i> , Procrustes variances are calculated for each set of observations (i.e.





201

202

203

204

205

206

207

208

209

210

211

212

213

214

215

number of observations (Adams 2016; Zelditch et al. 2012). We computed Procrustes variance for each combination of individual and device so that Procrustes variance reflectionly variation due to digitization. We then compared Procrustes variance between devices using a box plot and the permutational procedure implemented in geomorph. Next we quantified digitization consistency by computing repeatability for each device using the analogue of the intraclass correlation coefficient computed with the Procrustes ANOVA mean squares, as suggested by (Fruciano 2016). This value is normally comped between 0 and 1, with values close to 1 indicating much larger variation due to the factor used in computing the Procrustes ANOVA (in our case, variation among individuals) compared to residual variation (in our case, variation among digitizations). In other words, comparing repeatability between devices gives appliar information to the one obtained by the box plots of Procrustes variance but on a more easily interpretable scale from 0 to 1. We repeated our computations of repeatability for subsets of the data to test whether introducing semi-landmarks on curves and surfaces (patch points) changed the repeatability relative to a fixed landmark-only dataset. We did so for both 3D and µCT datasets to see if these trends differed by scan device. Finally, we investigated whether there is a difference between devices in a common task: the correct classification of sexual dimorphism (Fig. 2d). We began with a Procrustes ANOVA in R

replicates) as the sum of the diagonal elements of the set's covariance matrix divided by the

216

217

218

219

220

221

222

Finally, we investigated whether there is a difference between devices in a common task: the correct classification of sexual dimorphism (Fig. 2d). We began with a Procrustes ANOVA in R on the symmetric component for the subset of individuals with sex information (n = 11 distinct individuals; n = 66 3D models). This allowed us to gauge the magnitude of the effect of sexual dimorphism compared to other sources of variation, including variation due to scan device. Then with *Morpho*, we averaged the shape of each replicate triad for each device.



between-group PCA using sex as group (Boulesteix 2005). Between-group principal component analysis is an ordination technique which is gaining popularity in geometric morphometrics (eg. Firmat et al. 2012; Franchini et al. 2016; Franchini et al. 2014; Fruciano et al. 2016; Fruciano et al. 2014; Mitteroecker & Bookstein 2011; Raffini et al. 2018; Schmieder et al. 2015; Seetah et al. 2012) However, it can be also thought as a classification tool, as in the *Morpho* implementation which allows performing leave-one-out cross-validation. We, then used cross-validated classification accuracy as a measure of performance in classifying individuals based on their sex.

231 Results

#### **Analyses of shape variation**

Our Procrustes ANOVA results indicate that variation among individuals (%Var = 48.3) contributes the most to total variance, with asymmetry (directional and fluctuating), device, and operator error contributing the remainder (Table 1a). The %Var values indicate that directional asymmetry contributes a similar amount of variation as other sources of non-biological variation and that fluctuating asymmetry accounts for much less than digitization error and variation between devices (Table 1a). This means that using analyses of asymmetry with a combination of  $\mu$ CT and 3D surface scans would likely be unreliable in specimens the size of delicate mice or for specimens scanned at a similarly low resolution. The Procrustes ANOVA results for just the 3D data, confirms this observation in which digitization error is large compared to the components of asymmetric variation (Table 1b). For the 3D dataset, the error term (Res/Rep) contributes 17.8% of variation while asymmetry (Side) contributes 19.2%. In other words, for our 3D scan dataset, error contributes almost as much variation as asymmetry (Table 1b). The Procrustes ANOVA for just the  $\mu$ CT dataset, however, did not have this problem to the same





246	degree. Here, the error term (Res/Rep) contributes only 8.52% of variation while asymmetry
247	(Side) contributes 20.8% (Table 1c). In other words, error contributes less than one half of what
248	asymmetry contributes in the $\mu CT$ dataset. Therefore, a low resolution study of asymmetry with
249	3D scans would likely be unreliable unless appropriate arrangements are made to reduce error
250	(Fruciano 2016), whereas $\mu\text{CT}$ scans may be more suitable for these types of studies.
251	
252	The Procrustes ANOVA on just the symmetric component of shape reports the individual shape
253	representing biological variation, is 73.4% (Table 2). Differences between scan devices represent
254	14.6% and the residuals encompassing differences among replicates or operator error represent
255	12.0% of total variance (Table 2). Thus, our Procrustes ANOVA on the symmetric component
256	shows that most of the variation is due to biological sources but the significance of the variation
257	due to device may indicate systematic error.
258	
259	The PCA on the symmetric component revealed that the first three principal components (PCs)
260	account for $47.0\%$ of total variation (PC1 = $26.4\%$ , PC2 = $12.0\%$ , PC3 = $8.81\%$ , n = $114$ ) (Fig.
261	4). Each of the remaining PCs accounted for 6% or less of total variation therefore we only
262	considered the first three for the exploration of patterns of variation. Positive values along PC1
263	correspond to a larger braincase relative to the rostrum (Fig. 5a). Positive values along PC2
264	correspond to a wider frontal bone (Fig. 5b). Finally, positive values along PC3 correspond to a
265	more convex, dorsally-curved ventral surface (Fig. 5c).
266	
267	The plot of the scores on PC1 and PC2 supports the results from the Procrustes ANOVA on the
268	symmetric component of shape in that most of the visible variation is between individuals, i.e.



clusters of each individual's replicates (Fig. 4a). Indeed, regardless of scanning device, replicates from the same individual cluster together (Fig. 4a). For most individuals, replicates occupy non-overlapping regions of the plot except for those around the crowded mean shape near the origin (Fig. 4a). Within each individual's variation on PCA scores,  $\mu$ CT replicates usually form a tighter cluster than the 3D replicates (Fig. 4a). This pattern suggests that using  $\mu$ CT scans introduces less random error than using 3D scans. Furthermore, within an individual, 3D scan replicates tend to cluster closer to other 3D replicates while  $\mu$ CT scan replicates tend to cluster closer to other  $\mu$ CT replicates (Fig. 4a). Indeed, for most individuals, 3D scan replicates score lower than the  $\mu$ CT scan replicates from the same individual on both PC1 and PC2. These results suggest the systematic error may be driven by  $\mu$ CT scans overestimating both braincase volume and frontal bone width relative to 3D scans (Fig. 4a, Fig. 5a,b).

Overall, the scores along the first two PCs complement and provide an intuitive visualization for the patterns of higher error in 3D scans and of systematic error between the scan devices as

Overall, the scores along the first two PCs complement and provide an intuitive visualization for the patterns of higher error in 3D scans and of systematic error between the scan devices as observed in the Procrustes ANOVAs (Tables 1 and 2). The scores along PC1 and PC3 highlight another possible systematic difference between 3D and  $\mu$ CT scans (Fig. 4b). The PC3 axis displaces  $\mu$ CT replicates from 3D replicates such that variation in PC3 scores within individuals is often larger than variation in PC3 scores among individuals (Fig. 4b). On the PC3 axis, almost all 3D scan replicates had higher scores, which correspond to a more dorsally curved ventral surface relative to their corresponding  $\mu$ CT scan replicates (Fig. 4b, Fig. 5c).

#### **Procrustes variance and repeatability**





291	To compare the digitization error in each scanning device dataset, we calculated the Procrustes
292	variance among the replicate triads of each individual. We found that Procrustes variance is
293	significantly (p<0.001) higher in 3D scans (mean = $1.31x10^{-4}$ ) than in $\mu CT$ scans (mean =
294	4.76x10 <sup>-5</sup> ) (Fig. 6). This means that digitizations are more variable in 3D scans than in $\mu CT$
295	which is consistent with decreased clustering in 3D scans relative to $\mu\text{CT}$ scans in the PCAs (Fig.
296	4).
297	
298	The repeatability for each scan dataset mirrored the Procrustes variance results. We found that
299	the $\mu$ CT scan dataset had a repeatability of 0.896 and the 3D scan data had a repeatability of
300	0.750 (Table 3a,d). This means operators have an easier time repeating their digitizations (i.e.,
301	landmark placements) with $\mu CT$ scans than with 3D scans.
302	
303	To test how different types of landmarks impacted repeatability, we calculated repeatability for
304	combinations of landmark types for 3D and $\mu CT$ datasets consisting of only the symmetric
305	component of shape (Table 3). Because sliding landmarks depend on the placement of fixed
306	landmarks (and patch points depend on both fixed and semi-landlandmark curves), we could not
307	isolate each type of landmark's repeatability. The analyses restricted to completely manually
308	placed fixed landmarks always had the lowest repeatability of the three types of landmarks
309	(Table 3c,f). Repeatability was always highest for the datasets including all three types of
310	landmarks including the semi-automated semi-landmarks and the completely automated patch
311	points (Table 3a,d). Higher repeatability in datasets with the sliding landmarks may result
312	because the sliding smooths out user placement error across replicates.
313	



Analyses with a biological example: sexual dimorphism

A small subset of our dataset had sex information (n = 11; f = 7, m = 4), allowing us to perform a test on ether using different scan devices classify males and females according to shape with the same level of accuracy. Our Procrustes ANOVA on the symmetric component of shape variation using sex and device as factors found that shape differences due to device (Rsq = 0.0646) and sex (Rsq = 0.0952) are both significant (p < 0.001). Both factors have relatively small effect sizes, however, sex captures slightly more shape variation than device (Table 4). However, the between-group PCAs do not suggest marked sexual dimorphism to begin with (Fig. 7). Therefore, the subtlety of this biological signal could be the main reason for the small contribution of sex to total variation. Finally, we performed a cross-validation test on the between-group PCAs to assess which scan dataset can more reliably classify sexes based on shape (Table 5). The results show that in this case, 3D scans and  $\mu$ CT scans perform identically (overall classification accuracy = 63.6%).

328 Discussion

In this study, we contrasted very high resolution µCT scans with their extreme opposite: 3D surface scans of very small specimens. Our low versus high resolution datasets allowed us to assess whether the low resolution scans still allow defensible investigations of biological shape variation. We found that despite the low quality of the 3D scans, sufficient amounts of biological variation are present to perform, at the very least, typical interspecific comparisons. In datasets with only very slight intra-specific differences, more difficulties in distinguishing biological signal from error? Poise" may occur. For example, the subtle sexual dimorphism in our small sample was only just distinguished. However, we present three considerations to make before



using low resolution datasets. First, we found that variation due to scan device and digitizations substantial relative to asymmetric variation. This makes low resolution datasets a poor choice for studies on asymmetry. Second, using 3D scans creates more random error due to increased landmarking difficulty, therefore care should be taken in landmark choice, and possibly landmarking software and operator choice. Digitization error may also be reduced by taking averages of repeated measurements (Arnqvist & Martensson 1998; Fruciano 2016). Third, using 3D scans also introduces a source of systematic error relative to  $\mu$ CT scans, therefore we recommend not combining them whenever possible (see also Fruciano et al. 2017), and especially in studies on small intra-specific variation. In summary, with a few precautions listed above, we expect that for studies with similarly sized skulls or similarly low resolution scans, the variation due to error will be sufficiently low for successful detection of interspecific shape differences.

#### Measurement error and 3D scan reliability

Systematic error between the two scan devices is shown by consistent displacement patterns in the PCA. Indeed, across all three PC axes, the scans differ in how they measure concavity around the braincase, frontal, and ventral surface. This systematic pattern could suggest that the 3D scanner technology errs odding volume to the digital specimen relative to the  $\mu$ CT scan but it could also be the other way around with the  $\mu$ CT scan distorting the images to reduce volume. Furthermore, even when using the symmetric component of shape, the percent of variation contributed by scan device is quite substantial at about 14.5%. Because scan device contributes this much to variation and because systematic error between scan device exists, researchers





expecting very small variation due to biological sources would be advised not to combine 3D scan and  $\mu CT$  scan datasets.

361

362

363

364

365

366

367

368

369

370

371

372

373

374

375

376

377

378

359

360

While the two scan devices are usually comparable, using the low resolution 3D scans introduces more digitization error than the higher resolution μCT scans, which likely reflects increased user error due to lower resolution in 3D scans. This increased random error is reflected in both the larger point clouds of 3D replicates relative to µCT replicates in the PCAs, the higher Procrustes variance, and the lower repeatability score of 3D scans, particularly of manually-placed fixed landmarks. As expected, we found that the low resolution 3D scans were more difficult to landmark because key cranial features such as sutures and smaller processes were less distinct (Fig. 1). Nevertheless, our overall 3D scan repeatability score of 0.75 with symmetric data appears consistent with the literature: it is much lower than 3D scanned human-sized skulls – above 0.95 (Badawi-Fayad & Cabanis 2007; Fourie et al. 2011) but it is approaching the range of 3D scanned macropodoids (e.g., kangaroos) -0.78-0.98, depending on device and landmark choice (Fruciano et al. 2017). This trend of decreasing repeatability with decreasing body size may reflect measurement error becoming a larger percentage of overall size (Robinson & Terhune 2017). Relatedly, recent work has shown that excluding a few unreliable landmarks, or those with greater variability in placement, can significantly increase repeatability (Fruciano et al. 2017). This may be especially true for small specimens, for which small variations from the landmark location represent a larger percentage of their overall size.

379

380

381

Our repeatability tests on different combinations of landmark types suggest that fixed landmarks suffer the most from decreased resolution and the associated increased user error while patch





points suffer the least. We interpret these results to mean that the (semi-) automatic placement of semi-landmark curves and patches is more consistent in placing points compared to a human operator placing fixed landmarks, regardless of whether the automatic placement is "correct" or not. It is important to note that while semi-landmarks were "semi-automated", the user still manually defined the curve they slid along for each specimen. Furthermore, this curve is bounded by user-placed fixed landmarks. Therefore, the increased repeatability with increasing automation could also be due to the increased degrees of freedom afforded to landmarks during sliding: fixed with zero degrees, semi-landmarks with one degree, and patch points with two. The sliding, by removing variation tangential to a certain direction, will reduce the variance in those points which will appear to vary less so it would be expected that these points will contribute less overall variation when combined with the fixed landmarks.

This study did not look at multiple operator error which can be considerable, particularly if difficult landmarks are included (Fruciano et al. 2017). If inter-operator error were combined with the resolution-driven measurement error found here, it is possible that biological signal would diminish to a degree that could not support even interspecific comparisons.

# Measurement error introduced by scanning device compared to biological variation The challenge of any quantitative measurement study is to minimize measurement error introduced from various sources (in our case, device, resolution, and observer) relative to the "true" signal of biological variation. In the case of inter-observer error, which is one measurement error source, several studies suggest that interspecific variation can overwhelm



inter-observer such that this does not pose an issue with the correct interpretation of results (Robinson & Terhune 2017).

In our test on the ability of different scan devices to classify according to sexual dimorphism, we showed that while variation contributed by each source was similar (and that from scan device slightly lower), both scan datasets presented a small sexually dimorphic pattern and supported the same classification performance. This suggests that 3D scans may even be acceptable for detecting some intra-specific patterns. However, this was a small sample (n = 11) and further studies with larger datasets would improve confidence for using 3D scans for intra-specific studies. Studies based on larger datasets might also be able to better highlight differences in classification performance between devices, if any. Nevertheless, it is promising that 3D scans and  $\mu$ CT scans performed equally even at such a small sample size for such a subtle intraspecific signal.

Choosing a digitization device: 3D surface scanning versus µCT versus photogrammetry With many options for digitizing 3D specimens available, decisions on the acquisition mode must consider price, scanning time, processing time, portability, and scan resolution. The one-off investment of a relatively high resolution 3D surface scanner such as the HDI109 provided a model portable enough to take on airplanes and with fast scanning and processing times. Our model took 10 minutes from starting the scan to the finished surface file, but note that larger specimens requiring multiple sub-scans will take longer. These fast acquisition times are an asset in collection efforts that rely on expensive and time-limited museum travel. For example, one of us (AEM) digitized over 100 individuals in one week using the same scanning protocol.





427	However, the quality and speed of scanning varies by model; for example, other 3D surface
428	scanners could take over 45 minutes to capture one specimen and may also require more effort to
429	process scans (Katz & Friess 2014).
430	
431	Compared to 3D surface scanners, $\mu CT$ scanners provide much higher resolution, which in this
432	study translated into less measurement error. However, uCT facilities are not widely accessible,
433	not mobile, and tend to be more expensive. Depending on the facility, $\mu\text{CT}$ scanning involves
434	transport to the facility, scanning either by the operator, processing scans into image stacks, and
435	finally loading scans into specialized (and frequently high-cost) software to do the 3D
436	reconstruction. These reconstructions can be time consuming especially if the cranium needs to
437	be separated from the mandibles. Finally, specimens need to be loaned from their collections for
438	acquisition, which requires specimen transport and curator permission and is particularly
439	difficult when large numbers of specimens from distant locations need to be scanned.
440	
441	This study did not investigate photogrammetry, which is another and increasingly popular
442	method for digitizing 3D shape. This method uses software to align 2D photographs taken from
443	many different views into a 3D file. Photogrammetry is much cheaper and more portable than 3D
444	surface scanning since it only requires a camera of suitable resolution and very affordable photo-
445	alignment software like Agisoft PhotoScan (Agisoft LLC, St. Petersburg, Russia;
446	www.agisoft.com). The trade-offs are that in our experience, photogrammetry takes at least three
447	times longer to acquire the photos, it involves higher risk of human error or inconsistency during
448	photography, and it requires an order of magnitude more time to align the photos into a 3D
449	digital file. While photo-alignment can be done at convenience after photography, the greater





time required to capture enough photos may be a deciding factor for researchers with time limitations in museum collections. As for scan resolution, photogrammetry may perform better than 3D surface scanners in some cases (Fourie et al. 2011) or at least provide an acceptable alternative (Katz & Friess 2014; Muñoz-Muñoz et al. 2016).

Scan resolution is not the only consideration when choosing a scan device as its unique requirements for 3D model processing may increase image noise and therefore landmarking difficulty. Compared to scanning, 3D scans tend to be both noisier and require more model processing before 3D model export. Specifically, artificial smoothing and hole-filling may change the topography of the 3D mesh. Therefore, the comparison we have presented here is not just a comparison of resolutions but also a comparison of 3D model generation. The methods we provide in the supplementary files (Additional File 2: Supplementary Methods) represent the settings we found to decrease noise, however, the software also required some model smoothing and hole-filling before export. We recommend that researchers take these additional sources of image modification into account during their landmark choice and study design.

#### Conclusions

Here, we have shown that a 3D surface scanner can provide an acceptable alternative to a  $\mu$ CT scanner for assessing biological signal of 3D shape even in small specimens that are at the limits of 3D scanner resolution. Our analyses specifically showed that first, error contributes to a higher percentage of variation in 3D scan datasets than in  $\mu$ CT scan datasets of the same small specimens. As a result, we conclude that 3D scans are usually not appropriate for studies on very small sources of variation like fluctuating asymmetry. Second, we show that 3D scan datasets





have a lower repeatability of landmark placement, especially for fixed landmarks, as compared to  $\mu$ CT scans. Relatedly, our comparisons of repeatability on data with asymmetry to the same data without asymmetry – i.e. having bilateral symmetry – support analyzing the bilaterally symmetrical data of landmarks from low resolution scans. Finally, we use a preliminary study of sexual dimorphism to suggest that despite elevated error and shape variance, bilaterally symmetrical datasets from 3D scans can support male versus female classification based on small biological differences as well as  $\mu$ CT datasets can. In summary, while 3D scans are a promising alternative, exploratory pilot studies of measurement error like this one are advisable when practically possible (see also (Fruciano 2016).

Furthermore, the best 3D capture method will vary based on the study's design, expected effect size for the biological variation of interest, and the researcher's limitations on time, money, and travel. In addition to image resolution requirements, it is wise to assess the time it will take to capture and process each specimen as well as portability needs. We recommend a preliminary test on multiple devices – including surface scanners – to determine how levels of error compare to biological signal and whether there is substantial systematic error. Doing so may provide a defensible alternative to an expensive and time consuming large-scale acquisition of  $\mu$ CT scans including for studies on very small specimens.

#### **Acknowledgements**

We would like to thank Cruise Speck for assistance with Viewbox software and Dr. Heather Janetzki for hosting us in the mammal collections at the Queensland Museum.



196	Abbreviations
197	Landmark (LM)
198	Micro-computed tomography (μCT)
199	Principal component analysis (PCA)
500	Principal component (PC)
501	Three-dimensional (3D)
502	
503	References
504	Adams D, ML Collyer, and E. Sherratt. 2016. geomorph: Software for geometric morphometric
505	analyses. 3.0 ed.
506	Adams DC, and Otarola-Castillo E. 2013. geomorph: an r package for the collection and analysis
507	of geometric morphometric shape data. Methods in Ecology and Evolution 4:393-399.
808	10.1111/2041-210x.12035
509	Arnqvist G, and Martensson T. 1998. Measurement error in geometric morphometrics: Empirical
510	strategies to assess and reduce its impact on measures of shape. Acta Zoologica
511	Academiae Scientiarum Hungaricae 44:73-96.
512	Badawi-Fayad J, and Cabanis EA. 2007. Three-dimensional procrustes analysis of modern
513	human craniofacial form. Anatomical Record-Advances in Integrative Anatomy and
514	Evolutionary Biology 290:268-276. 10.1002/ar.20442
515	Boulesteix A-L. 2005. A note on between-group PCA. International Journal of Pure and
516	Applied Mathematics 19:359–366.
517	Breed B, and Ford F. 2007. Native mice and rats: CSIRO PUBLISHING.



518	Buser 1J, Sidlauskas BL, and Summers AP. 2017. 2D or Not 2D? Testing the Utility of 2D Vs.
519	3D Landmark Data in Geometric Morphometrics of the Sculpin Subfamily Oligocottinae
520	(Pisces; Cottoidea). The Anatomical Record.
521	Cardini A. 2014. Missing the third dimension in geometric morphometrics: how to assess if 2D
522	images really are a good proxy for 3D structures? Hystrix-Italian Journal of Mammalogy
523	25:73-81. 10.4404/hystrix-25.2-10993
524	Cornette R, Baylac M, Souter T, and Herrel A. 2013. Does shape co-variation between the skull
525	and the mandible have functional consequences? A 3D approach for a 3D problem.
526	Journal of Anatomy 223:329-336. 10.1111/joa.12086
527	Evin A, Horacek I, and Hulva P. 2011. Phenotypic diversification and island evolution of
528	pipistrelle bats (Pipistrellus pipistrellus group) in the Mediterranean region inferred from
529	geometric morphometrics and molecular phylogenetics. Journal of Biogeography
530	38:2091-2105. 10.1111/j.1365-2699.2011.02556.x
531	Firmat C, Schliewen UK, Losseau M, and Alibert P. 2012. Body shape differentiation at global
532	and local geographic scales in the invasive cichlid Oreochromis mossambicus. Biological
533	Journal of the Linnean Society 105:369-381. 10.1111/j.1095-8312.2011.01802.x
534	Fourie Z, Damstra J, Gerrits PO, and Ren YJ. 2011. Evaluation of anthropometric accuracy and
535	reliability using different three-dimensional scanning systems. Forensic Science
536	International 207:127-134. 10.1016/j.forsciint.2010.09.018
537	Franchini P, Colangelo P, Meyer A, and Fruciano C. 2016. Chromosomal rearrangements,
538	phenotypic variation and modularity: a case study from a contact zone between house
539	mouse Robertsonian races in Central Italy. Ecology and Evolution 6:1353-1362.
540	10.1002/ece3.1912



541	Franchini P, Fruciano C, Spreitzer ML, Jones JC, Elmer KR, Henning F, and Meyer A. 2014.
542	Genomic architecture of ecologically divergent body shape in a pair of sympatric crater
543	lake cichlid fishes. Molecular Ecology 23:1828-1845.
544	Fruciano C. 2016. Measurement error in geometric morphometrics. Development Genes and
545	Evolution 226:139-158. 10.1007/s00427-016-0537-4
546	Fruciano C, Celik MA, Butler K, Dooley T, Weisbecker V, and Phillips MJ. 2017. Sharing is
547	caring? Measurement error and the issues arising from combining 3D morphometric
548	datasets. Ecology and Evolution 7:7034-7046. 10.1002/ece3.3256
549	Fruciano C, Franchini P, Raffini F, Fan S, and Meyer A. 2016. Are sympatrically speciating
550	Midas cichlid fish special? Patterns of morphological and genetic variation in the closely
551	related species Archocentrus centrarchus. Ecology and Evolution 6:4102-4114.
552	Fruciano C, Pappalardo AM, Tigano C, and Ferrito V. 2014. Phylogeographical relationships of
553	Sicilian brown trout and the effects of genetic introgression on morphospace occupation.
554	Biological Journal of the Linnean Society 112:387-398.
555	Gunz P, Mitteroecker P, and Bookstein FL. 2005. Semilandmarks in Three Dimensions. <i>Modern</i>
556	Morphometrics in Physical Anthropology:73-98. 10.1007/0-387-27614-9_3
557	Katz D, and Friess M. 2014. 3D from standard digital photography of human crania—a
558	preliminary assessment. American Journal of Physical Anthropology 154:152-158.
559	Klingenberg C, Wetherill L, Rogers J, Moore E, Ward R, Autti-Rämö I, Fagerlund Å, Jacobson
560	S, Robinson L, and Hoyme H. 2010. Prenatal alcohol exposure alters the patterns of
561	facial asymmetry. Alcohol 44:649-657.
562	Klingenberg CP. 2011. MorphoJ: an integrated software package for geometric morphometrics.
563	Molecular Ecology Resources 11:353-357. 10.1111/j.1755-0998.2010.02924.x



564	Klingenberg CP, Barluenga M, and Meyer A. 2002. Shape analysis of symmetric structures:
565	Quantifying variation among individuals and asymmetry. Evolution 56:1909-1920.
566	Klingenberg CP, and McIntyre GS. 1998. Geometric morphometrics of developmental
567	instability: Analyzing patterns of fluctuating asymmetry with procrustes methods.
568	Evolution 52:1363-1375. 10.2307/2411306
569	Leamy LJ, and Klingenberg CP. 2005. The genetics and evolution of fluctuating asymmetry.
570	Annu Rev Ecol Evol Syst 36:1-21.
571	Mitteroecker P, and Bookstein F. 2011. Linear Discrimination, Ordination, and the Visualization
572	of Selection Gradients in Modern Morphometrics. Evolutionary Biology 38:100-114.
573	10.1007/s11692-011-9109-8
574	Munoz-Munoz F, and Perpinan D. 2010. Measurement error in morphometric studies:
575	comparison between manual and computerized methods. Annales Zoologici Fennici
576	47:46-56.
577	Munoz-Munoz F, Quinto-Sanchez M, and Gonzalez-Jose R. 2016. Photogrammetry: a useful
578	tool for three-dimensional morphometric analysis of small mammals. Journal of
579	Zoological Systematics and Evolutionary Research 54:318-325. 10.1111/jzs.12137
580	Muñoz-Muñoz F, Quinto-Sánchez M, and González-José R. 2016. Photogrammetry: a useful tool
581	for three-dimensional morphometric analysis of small mammals. Journal of Zoological
582	Systematics and Evolutionary Research.
583	Polychronis G, Christou P, Mavragani M, and Halazonetis DJ. 2013. Geometric Morphometric
584	3D Shape Analysis and Covariation of Human Mandibular and Maxillary First Molars.
585	American Journal of Physical Anthropology 152:186-196. 10.1002/ajpa.22340



586	Raffini F, Fruciano C, and Meyer A. 2018. Morphological and genetic correlates in the left-right
587	asymmetric scale-eating cichlid fish of Lake Tanganyika. Biological Journal of the
588	Linnean Society 124:67-84.
589	Reig S. 1996. Correspondence between interlandmark distances and caliper measurements.
590	Advances in Morphometrics 284:371-385.
591	Robinson C, and Terhune CE. 2017. Error in geometric morphometric data collection:
592	Combining data from multiple sources. American Journal of Physical Anthropology
593	164:62-75.
594	Rohlf FJ, and Marcus LF. 1993. A REVOLUTION IN MORPHOMETRICS. <i>Trends in Ecology</i>
595	& Evolution 8:129-132.
596	Rohlf FJ, and Slice D. 1990. Extensions of the Procrustes method for the optimal
597	superimposition of landmarks. Systematic Zoology 39:40-59. 10.2307/2992207
598	Schlager S. 2017. Morpho and Rvcg Shape Analysis in R. In: Guoyan Zheng SLaGS, ed.
599	Statistical Shape and Deformation Analysis: Academic Press, 217256.
600	Schmidt EJ, Parsons TE, Jamniczky HA, Gitelman J, Trpkov C, Boughner JC, Logan CC,
601	Sensen CW, and Hallgrimsson B. 2010. Micro-computed tomography-based phenotypic
602	approaches in embryology: procedural artifacts on assessments of embryonic craniofacial
603	growth and development. Bmc Developmental Biology 10. 10.1186/1471-213x-10-18
604	Schmieder DA, Benitez HA, Borissov IM, and Fruciano C. 2015. Bat Species Comparisons
605	Based on External Morphology: A Test of Traditional versus Geometric Morphometric
606	Approaches. Plos One 10. 10.1371/journal.pone.0127043



007	Sectan TK, Cardini A, and Miracle PT. 2012. Can morphospace shed light on cave bear spatiar-
608	temporal variation? Population dynamics of Ursus spelaeus from Romualdova pećina and
609	Vindija,(Croatia). Journal of Archaeological Science 39:500-510.
610	Shearer BM, Cooke SB, Halenar LB, Reber SL, Plummer J, Delson E, and Tallman M. 2017.
611	Evaluating causes of error in landmark-based data collection using scanners. Plos One
612	12:e0187452.
613	Sholts SB, Wärmländer SKTS, Flores LM, Miller KWP, and Walker PL. 2010. Variation in the
614	Measurement of Cranial Volume and Surface Area Using 3D Laser Scanning
615	Technology. Journal of Forensic Sciences 55:871-876. 10.1111/j.1556-
616	4029.2010.01380.x
617	Slizewski A, Friess M, and Semal P. 2010. Surface scanning of anthropological specimens:
618	nominal-actual comparison with low cost laser scanner and high end fringe light
619	projection surface scanning systems. Quartär 57:179-187.
620	Weisbecker V, and Goswami A. 2010. Brain size, life history, and metabolism at the
621	marsupial/placental dichotomy. Proceedings of the National Academy of Sciences
622	107:16216-16221. 10.1073/pnas.0906486107
623	Williams FL, and Richtsmeier JT. 2003. Comparison of mandibular landmarks from computed
624	tomography and 3D digitizer data. Clinical Anatomy 16:494-500. 10.1002/ca.10095
625	Yezerinac SM, Lougheed SC, and Handford P. 1992. MEASUREMENT ERROR AND
626	MORPHOMETRIC STUDIES - STATISTICAL POWER AND OBSERVER
627	EXPERIENCE. Systematic Biology 41:471-482. 10.2307/2992588



## **PeerJ**

528	Zelditch ML, Swiderski DL, and Sheets HD. 2012. Geometric Morphometrics for Biologists: A
529	Primer, 2nd Edition. Geometric Morphometrics for Biologists: a Primer, 2nd Edition:1-
630	478.
631	

# Figure 1

Low resolution 3D surface scans compared to  $\mu\text{CT}$  scans of the same delicate mouse crania.

3D scans of (A) dorsal view (B) lateral view and (C) ventral view compared to  $\mu$ CT scans of (D) dorsal view (E) lateral view and (F) ventral view. All crania are rendered in Viewbox v. 4.0.

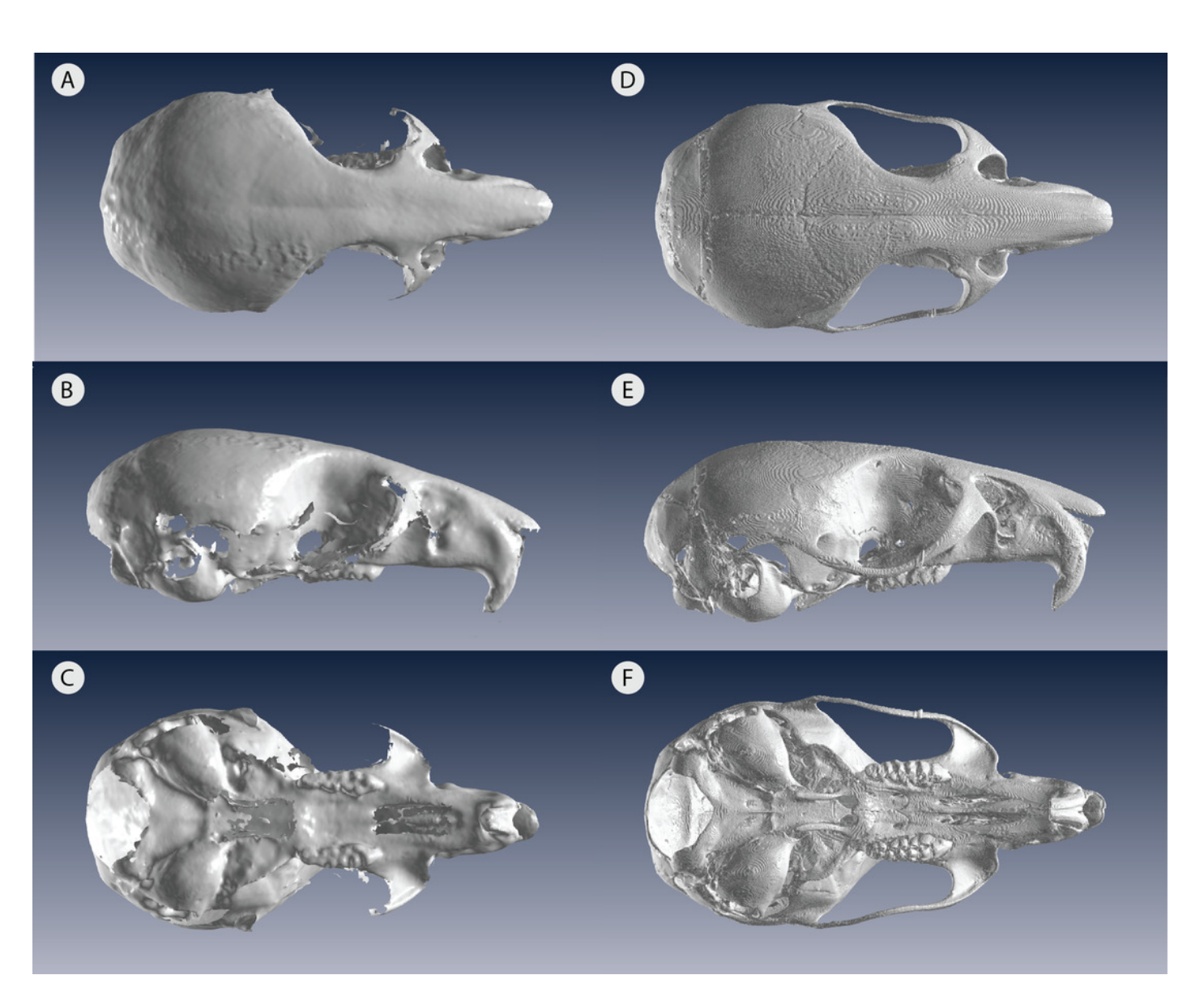
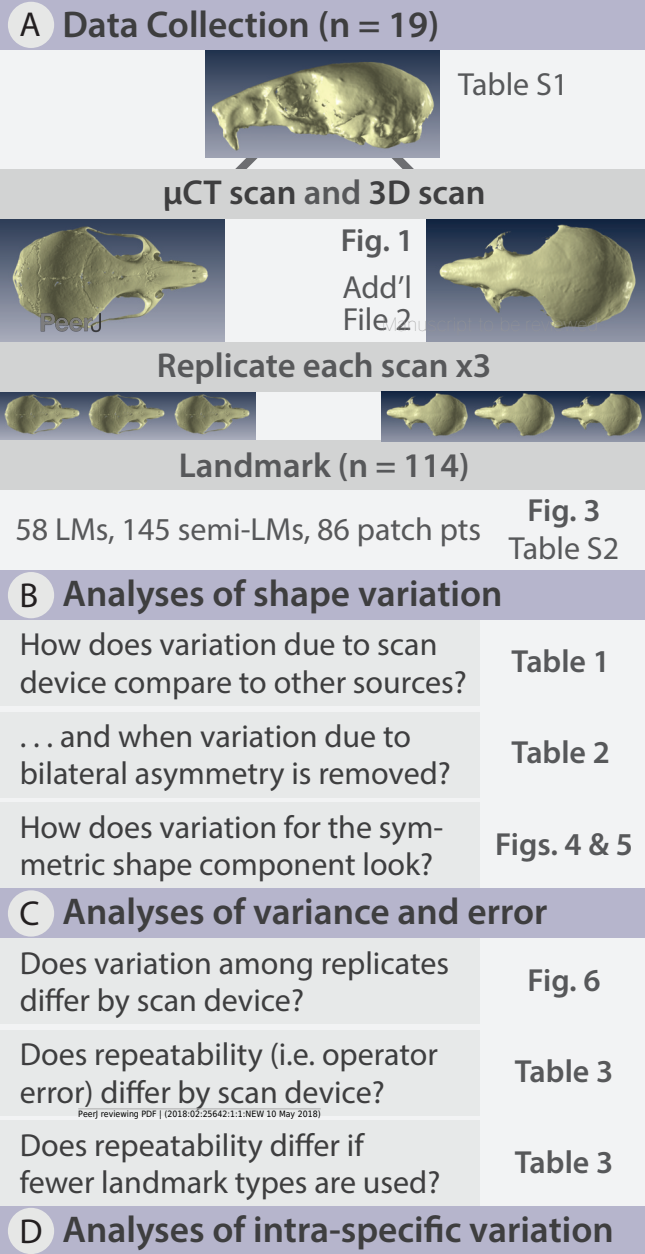




#### Figure 2(on next page)

Methods flow diagram highlighting the relationship between our questions and our analyses.

(A) All delicate mouse (*Pseudomys delicatulus*) crania were sourced from the Queensland Museum in Brisbane, Australia. Landmarks (LMs) capture homologous points, semi-landmarks (semi-LMs) capture curves between landmarks, and patch points capture surfaces between landmarks and semi-landmarks. (B - D) These sections of questions and associated figure and table numbers summarize how we organize the paper, particularly the Results, into three sets of related analyses.



How much sexual dimorphism

Table 4 appears to exist in our sample? Fig. 7

Does one scan device provide a better basis of sex identification?

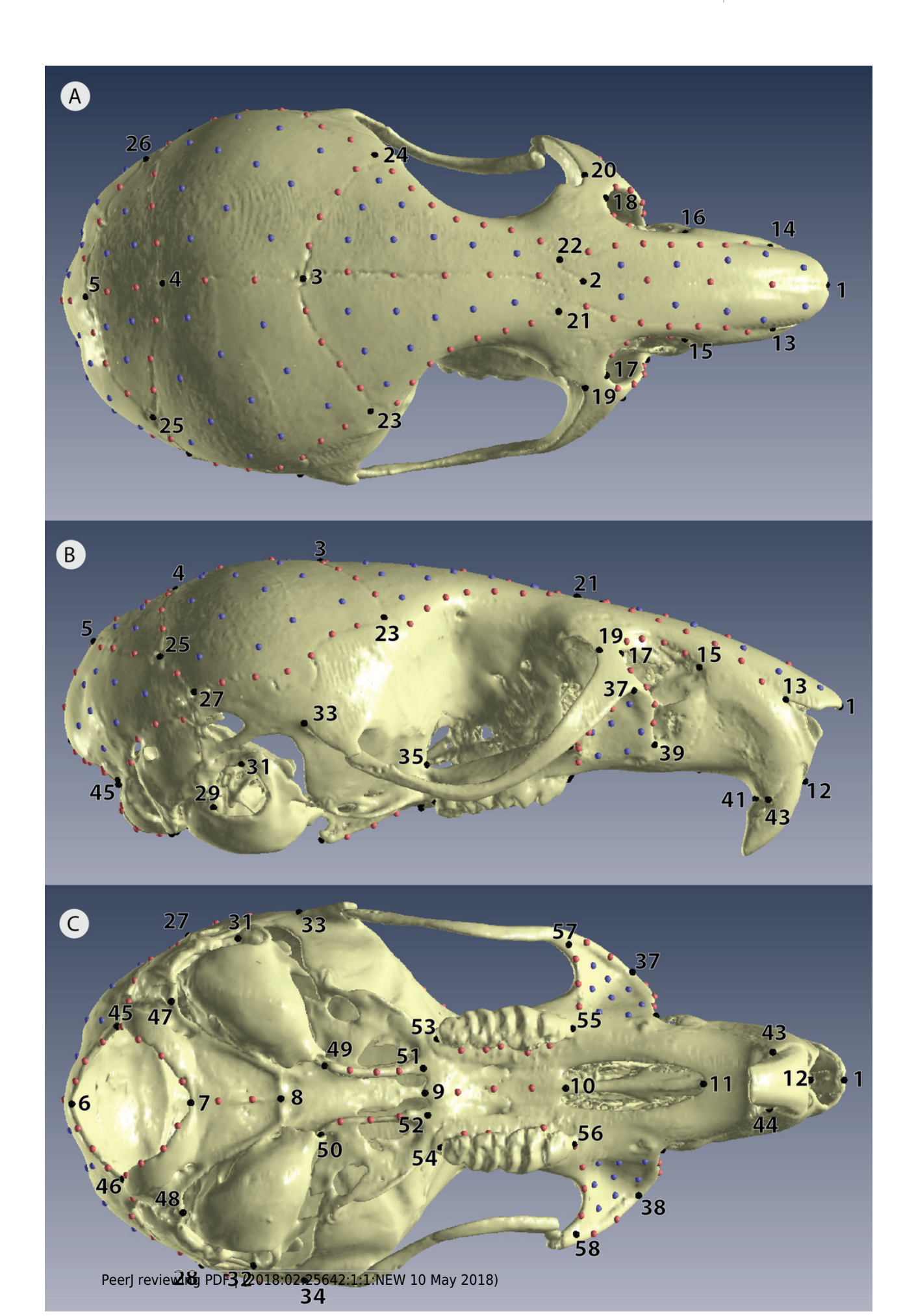
Table 5



# Figure 3

Positions of landmarks for geometric morphometric analyses.

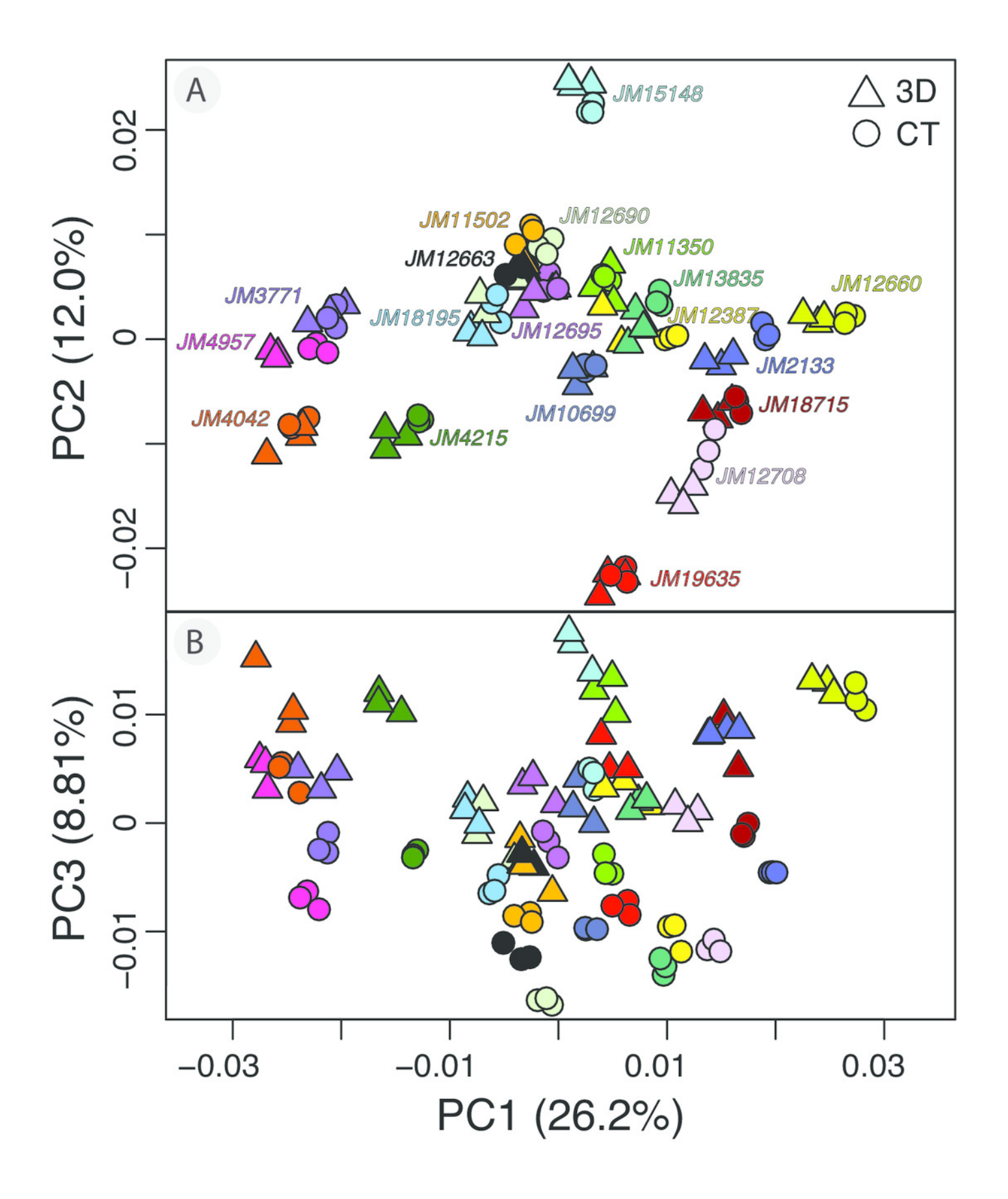
Locations of fixed landmarks (black points), sliding semi-landmarks (red points) and sliding surface patches (purple points) on a  $\mu$ CT scanned individual. (A) Dorsal view of the cranium. (B) Lateral view. (C) Ventral view. Definitions are given in Table S2.





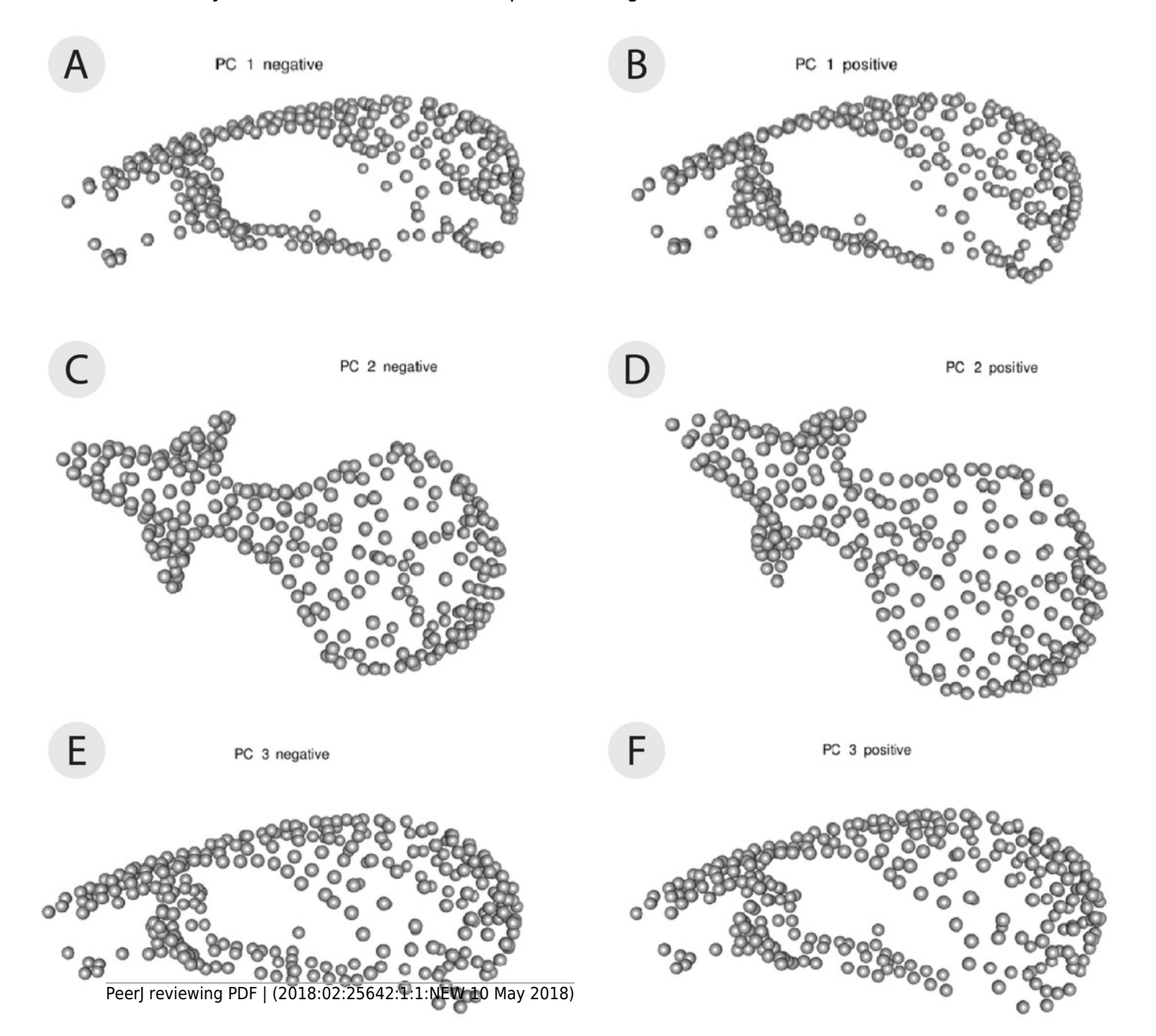
Exploratory PCA plots of shape variation showing differences among individuals, scan devices, and replicates of the same scan device.

(A) PC1 versus PC2 and (B) PC1 versus PC3. Each individual has a unique color shared by all of its 6 replicates. Each individual has 3 triangles to represent the 3D scanned replicates and 3 circles to represent the  $\mu$ CT scanned replicates. Each axis reports the total variance explained by that principal component.



3D warp-grids for the three most important principal components, showing minimum and maximum shapes for each PC.

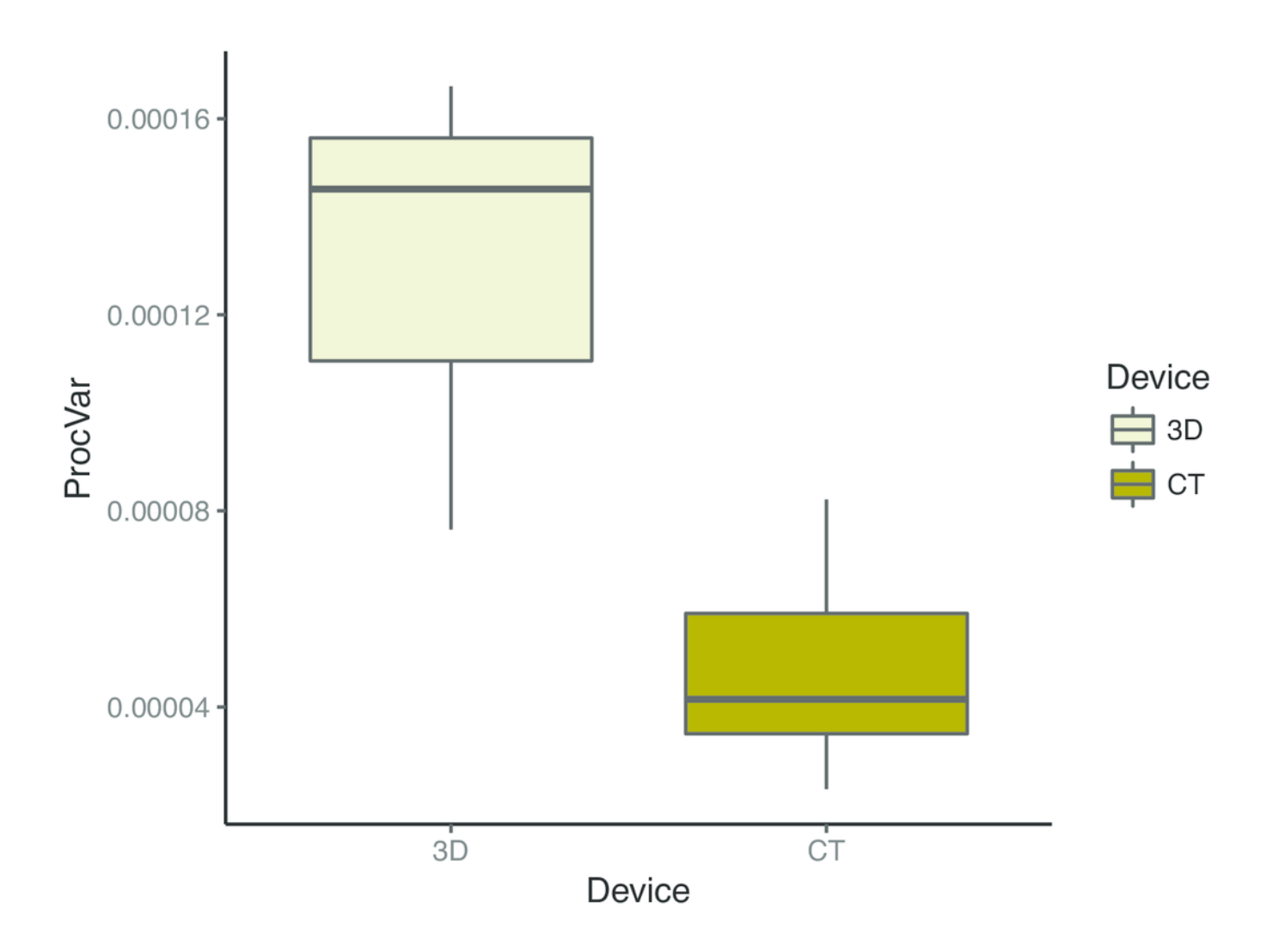
The right hand cranium shows the maximum positive shape for the principle component (PC) and the left hand cranium shows the minimum negative value. Compared to negative values (A), positive values along PC1 (26.4% variance) correspond to a larger braincase relative to the rostrum (B). Compared to negative values (C), positive values along PC2 (11.9% variance) correspond to a wider frontal bone compared to negative values (D). Compared to negative values (E), positive values along PC3 (8.9% variance) correspond to a more dorsally-curved ventral surface compared to negative values (F).





Morphological disparity -- as measured by shape variation among replicate scan triads -- by scanning device reflects operator error.

This box plot summarizes the morphological disparity (also known as the Procrustes variance) among the three replicates of an individual for each scan type. The mean Procrustes variance for 3D scans was  $1.34 \times 10^{-4}$  and  $4.81 \times 10^{-5}$  for  $\mu$ CT scans. This is a significant difference (p<0.001).





Intra-specific variation as shown by PCAs of 3D and  $\mu$ CT scan datasets colored by sex.

PCA provides an exploratory visualization of shape variation between males and females in our subsample with sex information (n=11). Males (n=4) are plotted in light blue and females (n=7) are plotted in dark red. Results from the cross-validation test can be found in Table 5.

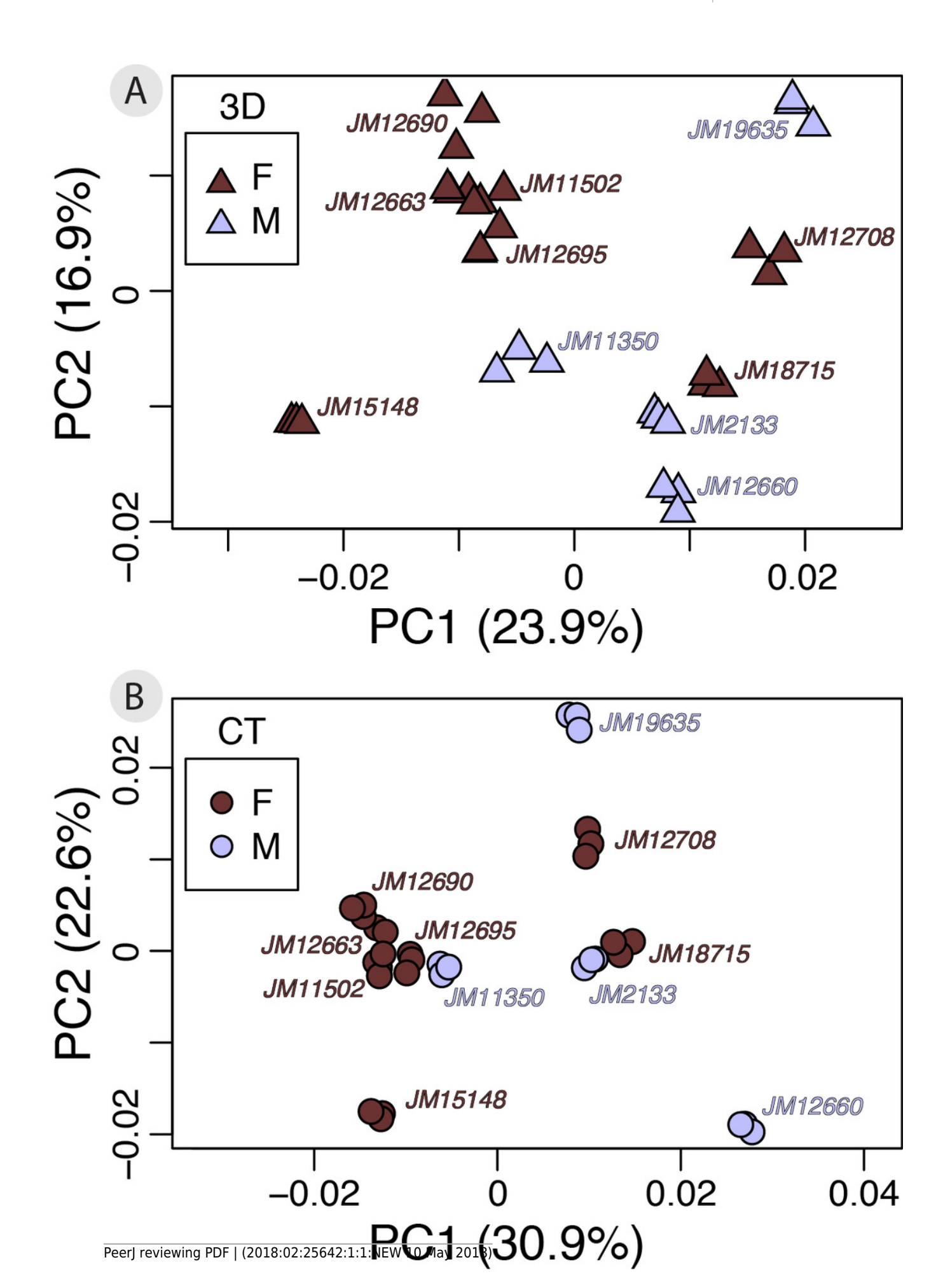




### Table 1(on next page)

General Procrustes ANOVA on sources of shape variation including asymmetry.

The %Var column of this Procrustes ANOVA demonstrates the relative contribution of each factor to overall variation. It is calculated from the sum of squares for each factor divided by the total sum of squares for all factors.

## **PeerJ**

1 A) All Specimens

11) 1111 S		1	1			
	Df	SS	MS	%Var	F	<b>Pr(&gt;F)</b>
Individual	8010	6.21E-02	7.76E-06	48.3	11.2	
						<.0001
Side	415	2.37E-02	5.70E-05	18.4	82.4	
						<.0001
Ind * Side	7470	5.17E-03	6.93E-07	4.02	0.54	1
Device	16340	2.08E-02	1.27E-06	16.1	4.90	
						<.0001
Res / Rep	65360	1.70E-02	2.59E-07	13.2		

2

B) Only 3D Specimens

, ,	Df	SS	MS	%Var	F	Pr(>F)
Individual	8010	3.52E-02	4.40E-06	51.6	4.24	<.0001
Individual	0010	3.32L-02	4.40L-00	31.0	7.27	\.0001
Side	415	1.31E-02	3.15E-05	19.2	30.4	<.0001
Ind * Side	7470	7.75E-03	1.04E-06	11.4	2.79	<.0001
Res / Rep	32680	1.22E-02	3.72E-07	17.8		

4 5

C) Only CT Specimens

C) Only	c i specimen	3				
	Df	SS	MS	%Var	F	<b>Pr(&gt;F)</b>
Individual	8010	3.45E-02	4.31E-06	61.7	6.41	<.0001
Side	415	1.17E-02	2.81E-05	20.8	41.8	<.0001
Ind * Side	7470	5.02E-03	6.72E-07	8.97	4.61	<.0001
Res / Rep	32680	4.76E-03	1.46E-07	8.52		



### Table 2(on next page)

Procrustes ANOVA on the sources of shape variation using the symmetric component of shape.

The R-squared column of this Procrustes ANOVA demonstrates the relative contribution of each factor to overall variation. The shape variation of this dataset is visualized in Figures 4 and 5.



	Df	SS	MS	Rsq	F	Z	Pr(>F)
ind	18	6.23E-02	3.46E-03	0.734	25.8	21.4	0.001
ind:Dev	19	1.24E-02	6.52E-04	0.146	4.86	23.7	0.001
Residuals	76	1.02E-02	1.34E-04	0.120			
Total	113	8.49E-02					



#### **Table 3**(on next page)

Comparison of operator error in 3D scan and  $\mu CT$  scan datasets using Procrustes ANOVAs and repeatability scores.

The repeatability score (R) is a value that reflects the ease of digitizing in a repeated measure study design. It is calculated from the Procrustes ANOVA using formulas for the intra-class correlation coefficient. The Procrustes ANOVAs were found by subsetting the dataset by scan device and by landmark types and then performing separate generalized Procrustes and bilateral symmetry alignments. (A-C) Results from the 3D-only dataset. (D-F) Results from the  $\mu$ CT-only dataset. (A) and (D) show the repeatabilites from the entire landmark datasets of each scan device. (B) and (E) remove patch points. (C) and (F) contain only fixed landmarks.



A) 3D Scan	All L	.andmark	s Includi	ng Patch	es (n = :	289)		
	Df	SS	MS	Rsq	F	Z	Pr(>F)	R
Ind	18	3.53E-	1.96E-	0.826	10.0	16.0	0.001	0.75
		02	03					0
Residuals	38	7.46E-	1.96E-	0.174				
		03	04					
Total	56	4.28E-						
		02						

B) 3D Scan Fixed Landmarks and Semilandmarks (n = 203)									
	Df	SS	MS	Rsq	F	Z	Pr(>F)	R	
Ind	18	4.37E-	2.43E-	0.807	8.826	16.7	0.001	0.723	
		02	03						
Residuals	38	1.04E-	2.75E-	0.193					
		02	04						
Total	56	5.41E-							
		02							

C) 3D Scan	C) 3D Scan Fixed Landmarks Only (n = 58)							
	Df	SS	MS	Rsq	F	Z	Pr(>F)	R
Ind	18	6.90E-	3.83E-	0.749	6.30	16.6	0.001	0.639
		02	03					
Residuals	38	2.31E-	6.09E-	0.251				
		02	04					
Total	56	9.21E-						
		02						

D) CT Scan	D) CT Scan All Landmarks Including Patches (n = 289)								
	Df	SS	MS	Rsq	F	Z	Pr(>F)	R	
Ind	18	3.46E-	1.92E-	0.927	26.9	18.4	0.001	0.896	
		02	03						
Residuals	38	2.72E-	7.15E-	0.073					
		03	05						
Total	56	3.73E-							
		02							

E) CT Scan Fixed Landmarks and Semilandmarks (n = 203)									
Df SS MS Rsq F Z Pr(>F)									
Ind	18	4.33E-	2.41E-	0.921	24.7	19.0	0.001	0.888	
		02	03						
Residuals	38	3.71E-	9.76E-	0.079					
		03	05						



Total	56	4.70E-			
		02			

F) CT Scan Fixed Landmarks Only (n = 58)								
	Df	SS	MS	Rsq	F	Z	Pr(>F)	R
Ind	18	6.28E-	3.49E-	0.893	17.6	20.2	0.001	0.847
		02	03					
Residual	38	7.54E-	1.98E-	0.107				
S		03	04					
Total	56	7.03E-						
		02						



### Table 4(on next page)

Symmetric Procrustes ANOVA with device and sex as factors to assess relative contribution of intra-specific variation to overall shape variation.

This Procrustes ANOVA allows comparison of the relative contribution to total variation from scan device and sex (R-squared column).



	Df	SS	MS	Rsq	F	Z	Pr(>F)
device	1	2.99E-03	2.99E-03	0.0646	4.84	4.06	0.001
sex	1	4.40E-03	4.40E-03	0.0952	7.14	4.96	0.001
Residuals	63	3.88E-02	6.16E-04				
Total	65	4.62E-02					



### Table 5(on next page)

Between group PCA classification test to assess whether one scan device dataset performs better at identifying sexes based on shape.

This analysis averages shape among replicates, computes a between-group PCA separately for 3D and  $\mu$ CT datasets, and runs a cross-validation classification test. The results indicate whether one type of scan dataset is more successful at classifying males versus females based on the shape variation present in the dataset. It also returns a kappa statistic; a kappa value over 0.20 indicates "fair" agreement between the two datasets. Shape variation visualized by sex can be seen in Figure 7.



Cross-validated classification results in frequencies		
3D	f	m
f (n = 7)	5	2
m (n = 4)	2	2
СТ	f	m
f (n = 7)	5	2
m (n = 4)	2	2
Cross-validated classification results in %		
3D	f	m
f	71.4	28.6
m	50.0	50.0
СТ	f	m
f	71.4	28.6
m	50.0	50.0
Overall classification accuracy (%)		
3D	63.6	
СТ	63.6	
Kappa statistic		
3D	0.214	
СТ	0.214	